Effect of detector geometry and surface finish on Cerenkov based time estimation in monolithic BGO detectors

Jens Maebe*[1] and Stefaan Vandenberghe[1]

[1]Department of Electronics and Information Systems, Ghent University, Ghent, Belgium

Abstract

Objective Time-of-flight positron emission tomography based on BGO detectors is made possible due to fast emission of Cerenkov light. Only around 17 Cerenkov photons are produced per 511 keV photoelectric event, making high photon collection efficiency crucial for obtaining good time-of-flight capabilities. In this study, we investigate how different lateral and back surface finishes affect the photon collection efficiency and Cerenkov based timing performance in monolithic BGO.

Approach The study is performed using GATE for gamma and optical photon modeling, with surface reflections of photons simulated by the LUT Davis model. We compare for different detector configurations (regarding size and surface finishes) the photon collection efficiency, detection delays of the first few optical photons and CTR estimations obtained by modeling the SiPM signals and performing leading edge discrimination. An additional comparison is made to LYSO scintillators and pixelated detectors.

Main results Although Cerenkov photon emission is directional, many high incidence angle Cerenkov photons are emitted due to electron scattering in the crystal. Substituting a polished back (photodetector side) surface for a rough surface increases the collection efficiency of these high angle of incidence photons. Results show that for a monolithic 50x50x12 $\mathbf{mm^3}$ BGO detector with reflective side surfaces, this leads to an overall increase in photon collection efficiency of 34%. Cerenkov photon collection efficiency is also improved, resulting in a reduction of the photon detection delays (and the variation therein) of the first few optical photons. This leads to a better coincidence time resolution, primarily achieved by a shortening of the tails in the time-of-flight kernel, with an 18% reduction in full width at tenth maximum.

Significance This study shows the importance of the photon collection efficiency for timing performance in Cerenkov based monolithic detectors, and how it can be improved with different surface finishes.

Keywords: time-of-flight positron emission tomography, TOF-PET, monolithic scintillation detector, Cerenkov, BGO

*Jens.Maebe@UGent.be

1 Introduction

Since the advent of time-of-flight positron emission tomography (TOF-PET), Bismuth Germanate (BGO) based PET detectors are no longer frequently used due to their slow scintillation decay time, leading to prohibitively low TOF resolutions. Most current PET scanners are therefore based on lutetium (yttrium) oxyorthosilicate, L(Y)SO, scintillation material given its superior scintillation characteristics compared to BGO, both in terms of light yield and decay time. BGO however recently had a resurgence in popularity due to Cerenkov based time estimation (Brunner and Schaart, 2017), made possible by improvements in silicon photomultipliers (SiPMs) and readout electronics. Cerenkov emission is nearly instant, but has a very low light yield. Only 17 photons are emitted on average per 511 keV event in pixelated BGO detectors (Gundacker et al., 2020). Therefore, improvements to photon detection efficiency, especially at shorter wavelengths where the majority of Cerenkov light is emitted, combined with the capability to detect individual photons at good time resolutions, played a big role in enabling time-of-flight capabilities for BGO.

Coincidence time resolution spectra of Cerenkov based PET detectors are however non-Gaussian in nature, with long tails produced by the statistical fluctuations in the number of detected Cerenkov photons. Image reconstruction may be improved by the use of multiple time-of-flight kernels, where each event is assigned a specific kernel based on its estimated time resolution (or estimated number of Cerenkov detections), significantly improving the image signal-to-noise ratio (Efthimiou et al., 2021). Characterizing events based on their time resolution can for example be achieved by sorting events by their signal rise time (Kratochwil et al., 2020). Studies on Cerenkov based time estimation in BGO have up until now however primarily been focussed on pixelated detectors.

There has also been a push towards monolithic PET detectors as they provide good spatial resolution using only a limited amount of electronic channels (compared to pixelated detectors of similar spatial resolution) and they intrinsically offer depth-of-interaction (DOI) information (Gonzalez-Montoro et al., 2021). Monolithic BGO detectors are currently being considered for use in the recently proposed Walk-Through Total-Body PET system (Vandenberghe et al., 2022). Rather than a horizontally positioned cylindrical geometry, it consists of two flat 70x105 cm^2 panels in an upright position, spaced 50 cm apart. The total-body (> 1 m) system is aimed to have a cost comparable to a standard clinical PET-CT system while reaching much higher sensitivity (only 33% lower than the Siemens Quadra) and offering full head plus torso imaging. This is in part made possible by the use of BGO, which has a higher stopping power, higher photofraction and is roughly 3 times cheaper than LYSO for the same volume. The number of readout channels and therefore the cost associated with SiPMs and other electronics is kept low by utilizing monolithic detectors. The long axial field of view and the close proximity of the two panels results in a high amount of oblique gamma photon incidences, for which the DOI decoding capabilities of monolithic detectors are crucial for accurate line-of-response (LOR) assignment.

The spatial resolution of monolithic detectors has been optimized quite well, providing especially good positioning performance when combined with deep learning, down to the 1 mm range in full width at half maximum (FWHM) (Stockhoff et al., 2021; Carra et al., 2022). Further improvements are unlikely to result in significant enhancement of image quality, as at this point the photon acolinearity and positron range start to become the dominant factors in LOR positioning. Enhancements to time resolution on the other hand lead to an increase in effective sensitivity and therefore signal to noise ratio of the reconstructed scans, providing more room for improvement.

In order to optimize the timing resolution, we should pay attention to the choice of surface finishes for the scintillator, as it can have a large impact on the photon transport characteristics and therefore affect the photon transfer times in the crystal (Berg, Roncali, and Cherry, 2015). In monolithic detectors, which have until now mostly been used in preclinical PET where TOF is not as important, these surfaces are often chosen to maximize spatial resolution. E.g. by using absorbing side surfaces to minimize reflections and thereby reduce edge effects. Optimizing for spatial resolution may however have an adverse effect on the time and energy resolution, by reducing the overall light collection efficiency. This is especially important for Cerenkov based time estimation, where we have to rely on the detection of a very small amount of photons for timing.

In this study, we perform a series of Monte Carlo simulations to better understand and evaluate the effect of detector geometry and scintillator surface finish on the photon collection efficiency and time resolution in monolithic BGO detectors. We additionally compare to LYSO scintillators, as well as pixelated detectors.

2 Method

We use GATE v9.2 (Sarrut et al., 2021), based on the Geant4 toolkit (Allison et al., 2016), to model gamma interactions in PET detectors and the subsequent production and transport of optical scintillation and Cerenkov light. We investigate both BGO and LYSO as scintillation material, with a variety of detector geometries (both monolithic and pixelated) and surface finishes.

The detector sizes under consideration are 50x50x16 mm^3, 50x50x12 mm^3, 25x25x16 mm^3 and 25x25x12 mm^3 for the monoliths. The 50x50x16 mm^3 size is chosen as starting point since it has the same aspect ratio as the smaller 25x25x8 mm^3 monolithic detectors already proven and currently in use in certain preclinical systems (Krishnamoorthy et al., 2018). It is also used in other monolithic detector studies (Stockhoff et al., 2021). A 12 mm thick version is additionally examined since making the switch from LYSO to BGO should allow for thinner detectors given the higher stopping power of BGO. The 25x25 mm^2 detectors are considered as an alternative option, as these smaller detectors would help with the count rate, especially important in total-body PET systems.

For each distinct detector configuration, we simulate 10 000 gamma photons impinging perpendicularly on the front surface of the detector, with entry points spread uniformely over the surface. Any generated optical photons are subsequently tracked, and those that are transmitted through the back surface (photodetector side) are recorded for further analysis.

The optical and scintillation properties of LYSO and BGO (Materials.xml file in GATE) are based on the data sheets provided by Epic Crystal (*LYSO(Ce) Scintillator* n.d.; *BGO Scintillator* n.d.), see Table 1. The wavelength dependency of the scintillation spectrum is taken into account for both scintillators, as well as the wavelength dependency of the refractive index for BGO. The refractive index for LYSO was chosen constant as it shows little change over optical energy ranges (1 eV - 5 eV). Surface reflections of optical photons are modeled by the LUT Davis Model (Roncali and Cherry, 2013), using custom look-up tables to represent different surface finishes.

2.1 Cerenkov production

Cerenkov light is produced when a charged particle, in this case a recoil electron ejected from its atom due to the energy deposited by the gamma photon, moves faster than the speed of light in a specific medium. The emission of Cerenkov light is directional, with photons emitted in a cone along the electron path. Despite this, Cerenkov photons emitted following a gamma interaction show relatively little correlation with the incoming gamma velocity vector. The electron itself is emitted in a cone along the direction of the incoming gamma photon, effectively increasing the maximum angle of Cerenkov emission. Furthermore, as the electron moves through the material, it constantly loses energy and changes direction due to collisions with other particles. This results in all but the first few Cerenkov photons to be emitted in fairly random directions relative to the gamma photon.

How quickly the electron loses 'directionality' is affected by the mean distance between collisions, also called the mean free path. Correct modeling of the electron path in Geant4 is therefore crucial for simulations regarding Cerenkov production. The default settings of GATE/Geant4 however lead to an overestimation of the mean free path, thereby resulting in overly focused Cerenkov photon emission angles (Trigila, Ariño-Estrada, et al., 2022). The mean step length of particles in Geant4 can be controlled by the $\Delta\beta$ parameter, which puts a limit on how much the kinetic energy of a particle is allowed to change during each step. We use $\Delta\beta$=0.02, resulting in a mean step length of $\approx$ 0.150 μm for 450 keV electrons in LYSO. This is close to the values of the mean free path of electrons in elemental solids with similar effective atomic number as LYSO (Shinotsuka et al., 2015), and is also an appropriate value to use for BGO (Trigila, Ariño-Estrada, et al., 2022).

Additionally, it should be taken into account that Geant4 does not automatically limit the Cerenkov emission spectrum to reasonable energy ranges, instead creating photons over the full energy range for which the refractive index n is specified (Dietz-Laursonn, 2016). We should therefore restrict the refractive index to transparent and physical energy regions for Cerenkov emission, where we use 310 - 850 nm for BGO and 390 - 750 nm for LYSO (Gundacker et al., 2020).

2.2 LUT Davis Model

The LUT Davis Model (Roncali and Cherry, 2013) allows to more accurately simulate reflection and transmission of optical photons at the interface between two materials by making use of measured 3D surface topographies. Given a surface sample, the model generates look-up tables (LUTs) containing the angular distribution of reflectance/transmittance, as well as the angular distribution of reflected and transmitted photons as a function of incidence angle. This is especially important when considering rough surfaces, where the reflectance/transmittance deviates greatly from the Fresnel equations, which are

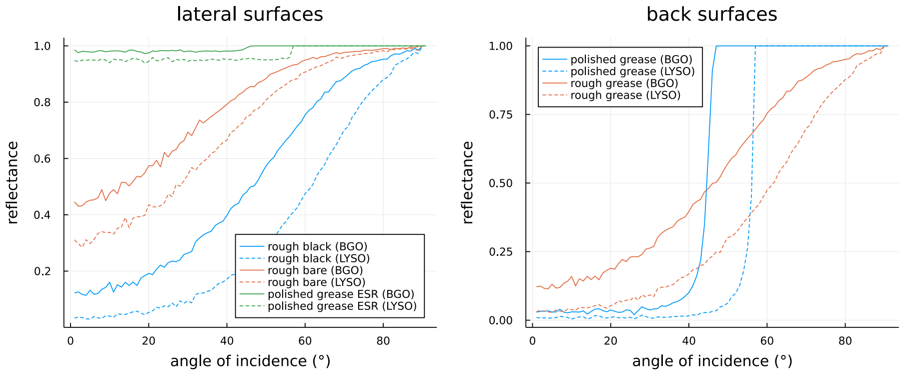

Figure 1: Angular distribution of reflectance of the surface look-up tables used throughout our simulations.

based on perfectly flat surfaces. The LUT Davis Model app (Trigila, Moghe, and Roncali, 2021) allows users to generate their own LUTs for use in GATE, by specifying the scintillation material (LYSO or BGO in our case), the surface finish (both a pre-existing polished and rough finish are available), the index of refraction of the coupling material (e.g. 1 for air or 1.5 for optical grease) and an optional reflector such as ESR. It should be noted here that the wavelength dependency of ESR is not taken into account, which may be non-negligible for Cerenkov emission due to the rapid drop-off in reflectivity below 370 nm. This is a limitation in the current LUT Davis model.

The different detectors considered in this study all use a polished front surface (opposite of the photodetector) coupled with optical grease to a specular reflector. We test three different lateral surfaces. The first is the exact same as the front surface (polished grease ESR), which is often found in pixelated detectors to maximize internal reflection. The second is a rough surface coated with black paint (rough black) to minimize reflections. It is modeled as a rough surface coupled with a material of refractive index 1.5 to a perfectly absorbing 'reflector'. This type of surface is often used in monolithic detectors to minimize side reflections and therefore reduce edge effects. The third lateral surface is a bare rough surface, so a rough surface coupled to air (rough bare). Finally, for the back surface we test both a rough and polished surface, both of them coupled with optical grease to the photodetector. Figure 1 shows the angular distribution of reflectance for the obtained LUTs.

2.3 Photon detection efficiency

As shown in Figure 1, not all photons reaching the back surface will be transmitted through to the actual SiPM surface. This results in the 'rejection' of a certain percentage of optical photons prior to any non-idealities unique to the photodetector itself. Of those transmitted photons, only a certain percentage will actually trigger an avalanche and therefore be detected, which is determined by the photon detection efficiency (PDE) of the SiPM in question.

In our simulations, we additionally take into account this (energy dependent) PDE of the SiPMs, for which we base ourselves on the Broadcom NUV-MT SiPMs (*AFBR-S4N66P024M 2×1 NUV-MT Silicon Photomultiplier Array*

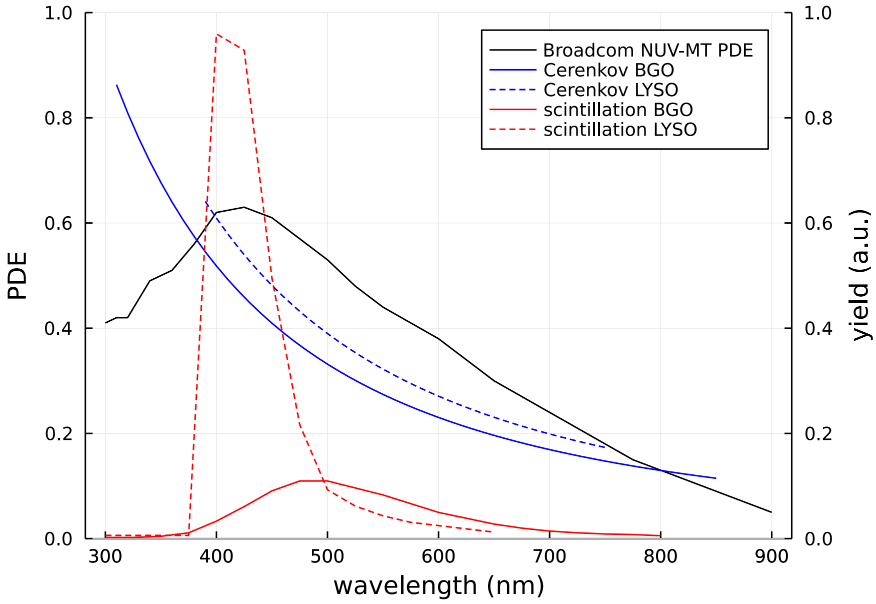

Figure 2: Photon detection efficiency (PDE) wavelength dependency of Broadcom NUV-MT SiPMs and Cerenkov/scintillation spectra of BGO and LYSO.

2022). These have a maximum PDE of 63% at a wavelength of 420 nm, and maintain over 40% PDE down to 300 nm. This makes them a good choice for Cerenkov photon detection, given that the Cerenkov emission spectrum scales with $1/\lambda^2$ and is therefore concentrated at lower wavelengths. Figure 2 shows the PDE overlaid with the Cerenkov and scintillation spectra of BGO and LYSO.

2.4 SiPM waveform simulation

As a final comparison, we will also estimate the coincidence time resolution of the different detector configurations by simulating the SiPM signals and predicting the gamma arrival time based on leading edge discrimination. The methodology for simulating the SiPM signals is inspired by (Acerbi and Gundacker, 2019), with simulation parameters again based on the Broadcom NUV-MT SiPMs (*AFBR-S4N66P024M 2×1 NUV-MT Silicon Photomultiplier Array* 2022).

The exact photon timestamps (both Scintillation and Cerenkov) as obtained from GATE are first assigned to their corresponding SiPM, randomly removing photons to account for the limited photon detection efficiency (wavelength dependent as before). In addition, dark counts are generated by sampling from a Poisson process at a rate of 4.4 MHz per SiPM. A photodetector transit time spread is then modeled by convolving the given timestamps with a Gaussian, where the standard deviation corresponds to the intrinsic single photon time resolution (SPTR) of the SiPM, calculated prior to the inclusion of electronic noise. A value of σ = 30 ps was used, estimated based on intrinsic SPTR measurements of similar SiPMs (Gundacker et al., 2020).

Next, prompt optical crosstalk with a certain probability (p = 23%) gives rise to duplicate counts, each of which can again result in crosstalk with the same probability. The i-th crosstalk event receives a time smearing $\sigma = SPTR\sqrt{i+1}$ with an additional time delay $\mu = SPTR\sqrt{i}$ (Acerbi and Gundacker, 2019). The SiPM signal $s(t)$ is then generated as a sum of tri-exponential functions centered around the photon detection times t_i, with rise time $\tau_{rise} = 100$ ps, fast decay time $\tau_{fast} = 5$ ns and slow decay time $\tau_{slow} = 55$ ns:

$$s(t) = \sum_i \left(C_{fast} \exp\left[\frac{t_i - t}{\tau_{fast}}\right] + (1 - C_{fast}) \exp\left[\frac{t_i - t}{\tau_{slow}}\right] - \exp\left[\frac{t_i - t}{\tau_{rise}}\right] \right) H(t - t_i) \tag{1}$$

The Heaviside function H sets the signal to zero prior to photon detection and C_{fast} ([0, 1], here 0.333) denotes the relative strength of the fast component of the decay time. The signal is then passed through a first-order low-pass Butterworth filter to simulate the limited bandwidth of the readout electronics. A cut-off frequency of 500 MHz was used, as is for example the case for the HRFlex-ToT ASIC, a readout ASIC compatible with monolithic detectors (Sánchez et al., 2022). Finally, electronic noise is added to the signal as zero-mean white Gaussian noise with $\sigma = 5\%$ of a single photoelectron pulse amplitude.

3 Results

3.1 Photon collection efficiencies

Figure 3 shows the photon collection efficiency (optical photons detected per event) of BGO and LYSO for two detector geometries, 50x50x12 mm^3 monolithic and 3x3x20 mm^3 pixelated, with different lateral and back surface finishes. Only events with full (511 keV) energy deposit in the crystal are considered, including both scatter + photoelectric and purely photoelectric events. Note that the PDE of the SiPMs is already included in these results.

As was observed in Figure 1, a rough back surface allows detection of more high incidence angle photons, at the cost of reduced transmission at lower incidence angles. Since scintillation photons are emitted isotropically in 3 dimensions, the angular distribution relative to the photodetector surface normal is proportional to the radius of the corresponding circle on the unit sphere. This results in more emission of high incidence angle photons. For monolithic detectors, or when using reflective side surfaces, the rough back surface results in a net gain of photon collection efficiency since many of these high angle photons do in fact make it all the way to the photodetector surface. For the monolithic BGO detector with reflective side surfaces, the rough back surface leads to a 34% increase in photon collection efficiency compared to a polished back surface. We also observe that the differences are larger in BGO than in LYSO, since the higher index of refraction of BGO (2.15 compared to 1.82 for LYSO) leads to a larger mismatch with the optical grease.

The same trends can be seen for the Cerenkov photons specifically as well. The combination of the short mean free path of the electron, the fact that the recoil electron itself will not be emitted in the exact same direction as the incoming gamma photon, and the possibility of the gamma photon itself having been scattered, results in many high incidence angle Cerenkov photons. A median of only 2 Cerenkov photons is detected per event for a rough black lateral surface with a polished back surface, whereas using a polished reflective lateral surface with a rough back surface increases this to a median of 5 Cerenkov photons.

Figure 4 shows the same results but for different monolithic BGO detector sizes. The overall trends remain the same, with the larger and thinner detectors generally showing higher photon collection efficiencies. For these detectors, there is a smaller probability of losing photons to the lateral surfaces.

3.2 Photon detection delays

In Figure 5 we take a look at the photon detection delays, which is the time between the gamma photon passing through the front surface of the detector and the detection of the n-th optical photon. A higher photon collection efficiency generally results in earlier photon detections. This is most obvious for the pixelated detectors, which overall had the lowest photon collection efficiencies. On the other hand, when there were many photons detected to begin with, as is the case for monolithic LYSO, further enhancing the photon collection efficiency has little to no effect.

The absolute values of the photon detection delays however do not have any direct impact on the coincidence time resolution (CTR), since these cancel out for two identical detectors in coincidence. More important is the spread on the detection delays, especially in those cases where we rely on single photon detection per SiPM, as is the case for monolithic BGO. We see here that the rough back surface results in earlier photon detections with less variation, with the best results being obtained when combined with reflective lateral surfaces.

How fast the photons are coming in one after another (i.e. the slope in Figure 5) may also have an effect on the CTR. This is primarily relevant when there are sufficient detections per SiPM for the signals to quickly pile up (e.g. for pixelated detectors), increasing the slope dV/dt of the SiPM signal and therefore reducing noise on the leading edge discrimination (Jarron et al., 2009).

3.3 CTR estimations

We estimate the CTR of the monolithic detectors by simulating the SiPM signals and predicting the gamma arrival time based on leading edge discrimination. For the 50x50 mm^2 detectors we use an 8x8 readout of 6x6 mm^2 SiPMs, and for the 25x25 mm^2 detectors a 4x4 readout of the same 6x6 mm^2 SiPMs. Leading edge discrimination is performed on each individual SiPM waveform, resulting in a matrix of 8x8 or 4x4 timestamps. We use a leading edge discrimination threshold of 0.5 photoelectron pulse amplitudes in order to detect individual Cerenkov photons. Due to the presence of dark counts, the signal amplitude prior to gamma detection is not necessarily centered around 0 and may even be above the 0.5 photoelectron threshold level. This leads to a fraction of the SiPMs recently having triggered prior to the actual gamma event, resulting in 'dead' SiPMs incapable of triggering again for a certain time. We therefore lose the timing information of those SiPMs. In our simulations this limitation was modelled by considering those SiPMs with a signal amplitude > 0.25 photoelectrons prior to the gamma event as dead, and therefore not being present in the timestamp matrix.

The gamma arrival time itself was then predicted as the first SiPM timestamp. Averaging of the first few timestamps was also tested, but consistently

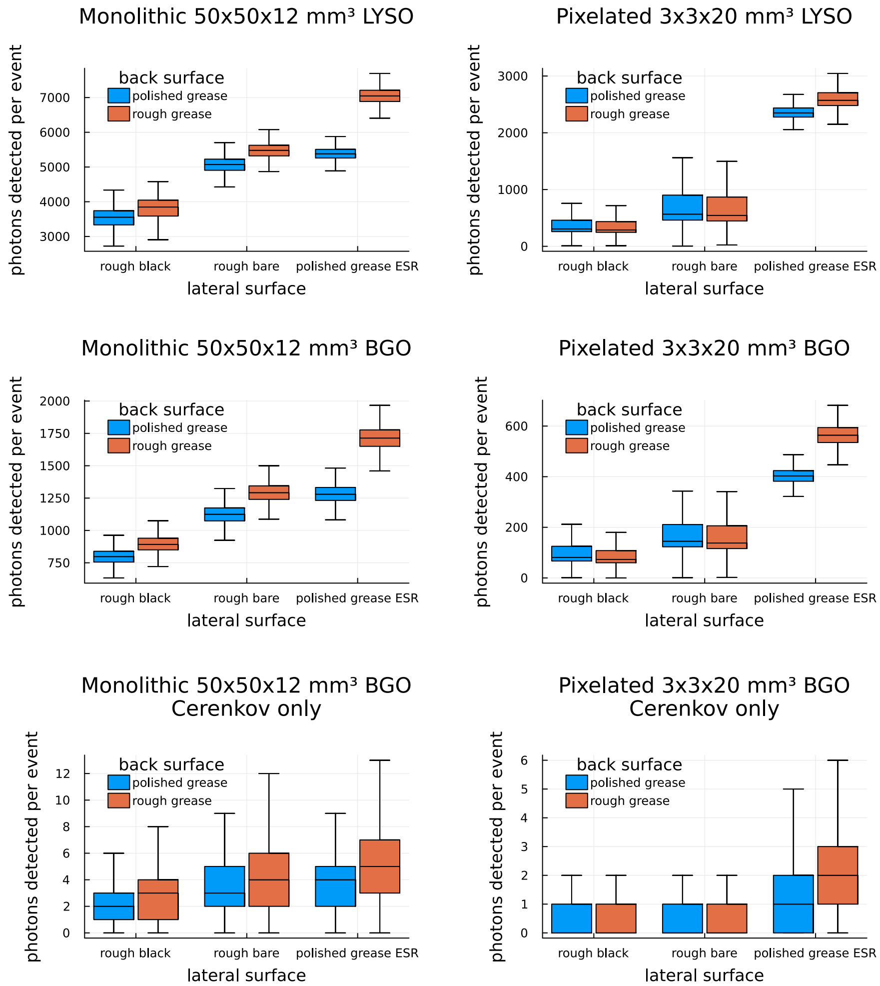

Figure 3: Comparison of photon collection efficiency for different surface finishes in monolithic and pixelated BGO and LYSO detectors. The top two rows consider both scintillation and Cerenkov photons, whereas the bottom row looks only at Cerenkov photons in BGO.

	unit	LYSO	BGO
scintillation yield	1/MeV	29 000	8 500
energy resolution	%	10.9	11.9
rise time	ps	70	70[a]
decay time	ns	42	317
emission peak wavelength	nm	420	480
refractive index		1.82	2.15[b]

Table 1: Material properties of LYSO and BGO used in the GATE simulations. The energy dependency of the scintillation spectra is taken into account for both materials, as well as the wavelength dependency of the refractive index for BGO.
[a]Value was not provided in the datasheet so it was chosen equal to LYSO for the comparison. It is nonetheless in line with experimental results (Brunner and Schaart, 2017).
[b]At the emission peak wavelength.

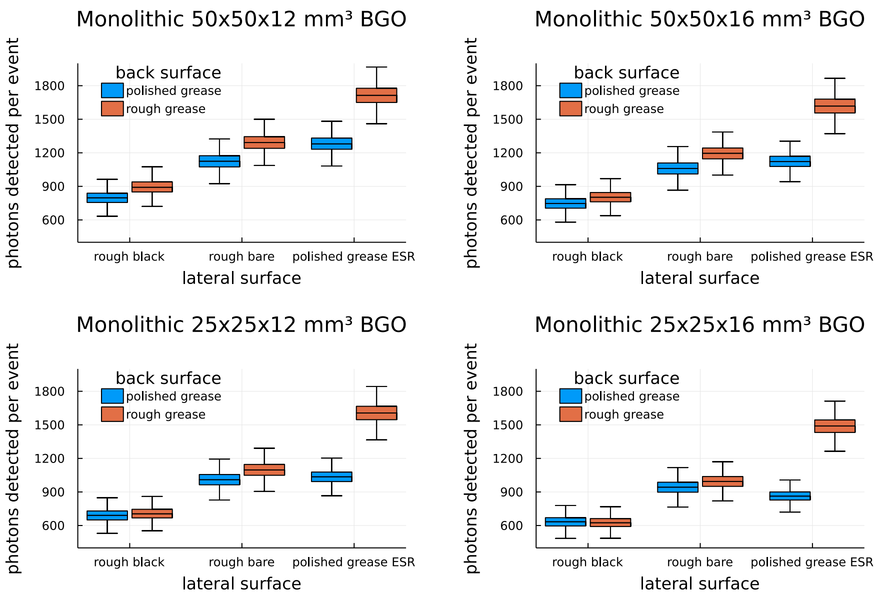

Figure 4: Effect of surface finish on photon collection efficiency in different monolithic BGO detector sizes.

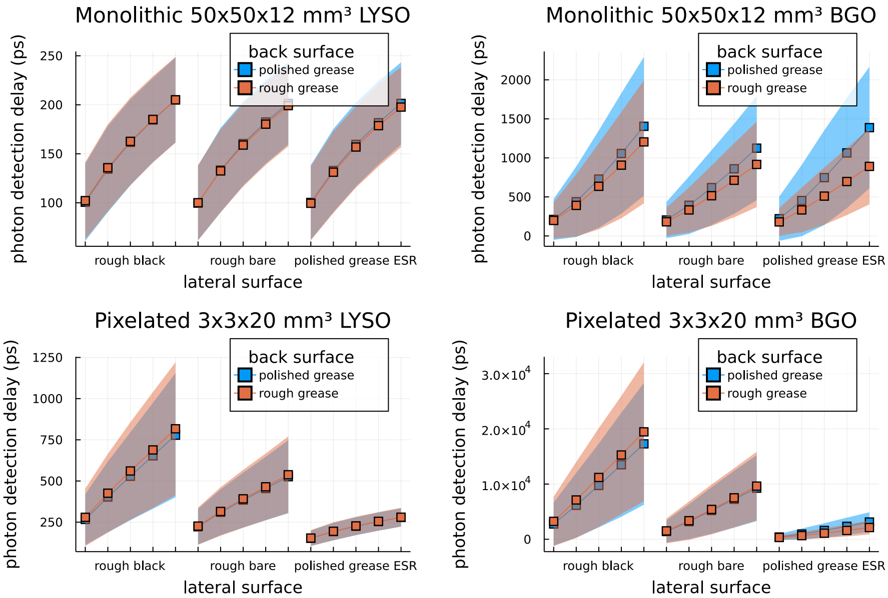

Figure 5: Time delay between the gamma photon passing through the front surface of the detector and the detection of the n-th photon (increasing left to right from n=1 to n=5). Values are averaged over all events of a specific configuration, with confidence intervals showing the standard deviation ($\pm\sigma$).

underperformed for monolithic BGO. The TOF kernels are constructed by randomly subtracting different events from one another (to obtain events in coincidence), after which a kernel density estimation fit is performed to obtain a distribution from the TOF histogram. Figure 6 shows such a TOF kernel for a case with long tails (monolithic 50x50x16 mm^3 BGO with rough black sides and a polished detector surface). The kernel density estimation fit is compared to a Gaussian with the same FWHM, showing the non-Gaussian nature of the TOF kernel.

Figure 7 shows the coincidence time resolutions for the different monolithic detector configurations. Here we have used a leading edge discrimination threshold of 0.5 photoelectron pulse amplitudes. Since the distributions are not perfectly Gaussian, we report the full width at half maximum (FWHM/FW2M), full width at tenth maximum (FWTM/FW10M) and the full width at twentieth maximum (FW20M). While the FWHM remains in the same range for the different configurations, the FW10M and FW20M show larger differences. That is, the different surface finishes mostly affect the tails of the distribution. The thinner (12 mm) crystals provide a better time resolution, with the rough back surface resulting in lower FW10Ms and FW20Ms (shorter tails), especially when using non-absorbing lateral surfaces. E.g. for monolithic 50x50x12 mm^3 BGO with reflective side surfaces, we see a reduction of 18% in FW10M going from a polished back surface to a rough back surface. Again we also see that for monolithic LYSO, the surface finish has negligible impact on the coincidence time resolution.

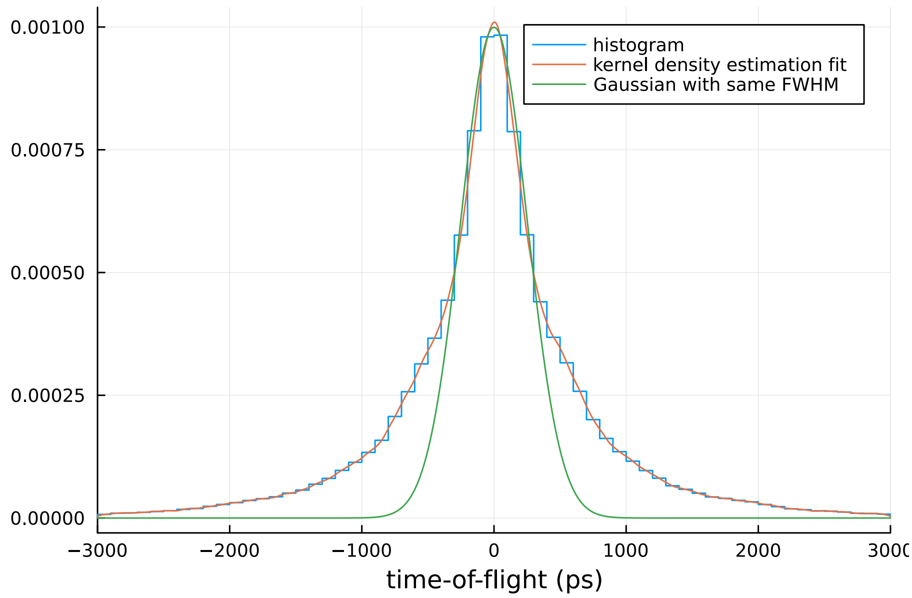

Figure 6: Time-of-flight kernel of monolithic 50x50x16 mm³ BGO with rough black sides and a polished detector surface. The kernel density estimation fit, which accurately describes the time-of-flight histogram, is compared to a Gaussian kernel with the same FWHM, showing the extent of the tails.

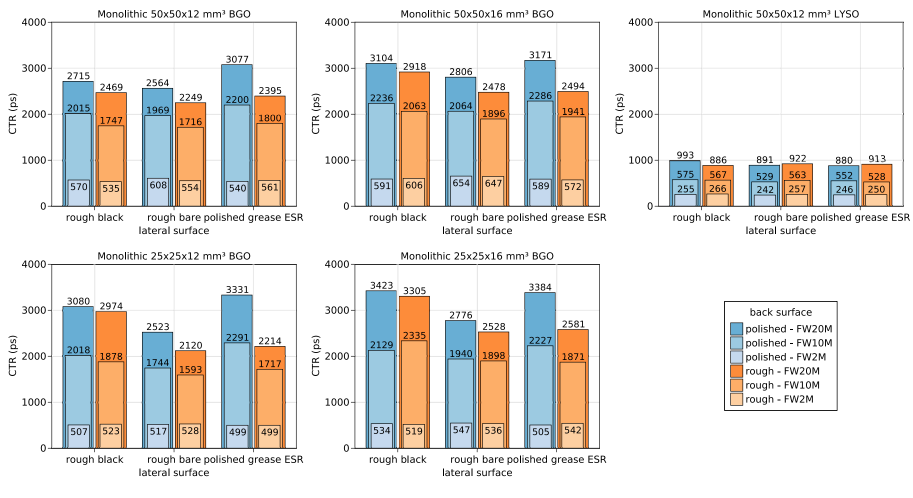

Figure 7: Coincidence time resolution obtained by leading edge discrimination for the different detector configurations.

4 Discussion

In order to benefit from Cerenkov based time estimation, it is important to use SiPMs and readout electronics that are in fact capable of resolving individual photon detections. Note that only a few Cerenkov photons are detected per event for an entire 50x50x12 mm^3 monolithic BGO detector (Figure 3), over a total of 64 SiPMs. Given the large spread in Cerenkov emission angles, it is highly improbable that more than one Cerenkov photon will be detected by the same SiPM and we can therefore not rely on fast signal pile-up. Modern SiPMs can easily detect individual photons, and readout electronics have no problem detecting the leading edge of an SiPM signal below a single photoelectron level. The difficulty lies in the generation of dark counts, which can lead to missing Cerenkov photon detections or dark counts being misinterpreted as a Cerenkov photon.

4.1 Effect of dark counts

In order to detect (sufficient) Cerenkov photons in monolithic detectors, it is required to set the leading edge threshold below a single photoelectron level. The SiPMs will rarely trigger on Cerenkov photons at higher thresholds, since most SiPMs detect no more than a single Cerenkov photon. While the dark count rate of a single SiPM is not that high (4.4 MHz), we are dealing with 64 SiPMs for the 50x50mm^2 detector configurations. This means that on average, we detect a dark count every $\sim$3.6 ns over the whole detector, which is only an order of magnitude larger than the typical coincidence time resolutions.

An SiPM that is triggered by a dark count will be incapable of triggering again for a short time while the signal amplitude drops off. If a Cerenkov photon happens to be absorbed during this timeframe, it will still contribute to the SiPM signal, but no leading edge detection will trigger. These 'dead' SiPMs essentially equate to a loss of photon collection efficiency when it comes to timing information. In addtion, while most dark count triggers can be rejected based on energy integration, measuring a dark count every $\sim$3.6 ns means that there is a non-negligible probability that a dark count occurs just prior to the gamma event. It would therefore be indistinguishable from a Cerenkov photon, leading to a false datapoint in the timestamp matrix.

Dark counts are likely less problematic in pixelated detectors, since the overal dark count rate is lower (only one SiPM per pixel) and all Cerenkov photons are detected by the same SiPM, so that a higher leading edge threshold would still be capable of detecting Cerenkov photons. This is still partially true of monolithic LYSO, where many photons reach the SiPMs sufficiently quick one after another to still obtain valuable time information using thresholds above the single photoelectron level. Therefore, further reductions in dark count generation of SiPMs, and readout electronics better capable of dealing with dark count rejection are especially important for timing in monolithic BGO.

4.2 Effect of photon collection efficiency

The photon collection efficiency of the detectors plays a significant role in timing performance when relying on Cerenkov photons for time-of-flight estimation. We can appreciate this in Figure 7, consistently showing better time resolutions for the higher photon collection efficiencies. The detectors with higher photon collection efficiencies do detect more high incidence angle (for the rough back surface) or reflected (for the reflective lateral surfaces) photons. These photons have longer (and higher variation in) photon transfer times from the gamma interaction position to the photodetector. Therefore, accurate prediction of the transfer time of an individual photon is more difficult. Nonetheless, these detectors show better overall timing statistics due to the larger amount of photon detections.

4.3 Time-of-flight kernels

As mentioned, the photon collection efficiency in monolithic BGO primarily has an effect on the tails of the time-of-flight kernel, showing shorter tails for higher collection efficiencies. Figure 8 shows the time-of-flight kernel (as was obtained in Figure 7) for a low and high photon collection efficiency configuration of monolithic 50x50x16 mm^3 BGO: absorbing lateral sides with a polished back surface, and reflective lateral sides with a rough back surface. The longer tails can be attributed to more events with fewer Cerenkov detections.

A similar effect can be seen when comparing purely photoelectric with scattered (but still 511 keV) events, showing considerable time resolution degradation for scattered events. The effect is now no longer confined to the tails, increasing the FWHM from 465 ps for purely photoelectric events to 817 ps for scatter + photoelectric events. This is due to a reduced emission of Cerenkov light. Simulations of the monolithic 50x50x16 mm^3 BGO detector show only 10 Cerenkov photons emitted on average per scatter + photoelectric event, compared to 18 photons for purely photoelectric events. Note that this poses less of a problem for pixelated detectors, where the majority of 511 keV events are purely photoelectric since a scattered gamma photon often exits the crystal before depositing the rest of its energy. For monolithic detectors though, scattered events will not only contribute to a degradation of spatial resolution, but also time resolution.

Identification of scattered events could however allow for image reconstruction with multiple time-of-flight kernels, improving overall image signal-to-noise ratio (Efthimiou et al., 2021). Scatter identification was for example done for LYSO with a deep learning based approach using simulated data (Decuyper, Milan, 2021). The difficulty here lies in using a network trained on simulated data for experimental data. Additionally, BGO has shorter range scatters compared to LYSO, which makes them more difficult to identify. Therefore, the feasibility of such an approach would require further investigation.

Another approach for time-of-flight kernel separation would be identifying events with good timing based on the SiPM signal rise time, as was previously done in pixelated BGO detectors (Kratochwil et al., 2020). This would likely require summing of the SiPM signals in monolithic detectors, since most Cerenkov photons are absorbed by different SiPMs and the signal rise time of individual SiPMs is therefore unlikely to vary much. It should nonetheless be possible to implement for monolithic detectors, providing an additional method to improve image signal to noise ratio for a given detector configuration.

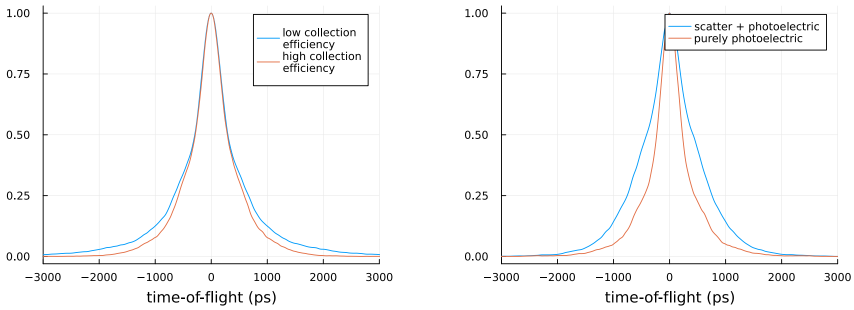

Figure 8: Time-of-flight kernels for monolithic 50x50x16 mm^3 BGO. **Left**: two different surface finish configurations, one with low photon collection efficiency (rough black lateral and polished back surface) and one with high photon collection efficiency (polished reflective lateral and rough back surface). **Right**: comparison between purely photoelectric and scatter + photoelectric events for the high photon collection efficiency configuration.

5 Conclusion

This study shows the importance of optimizing the photon collection efficiency to improve Cerenkov based time estimation in monolithic BGO detectors. Multiple detector configurations were simulated for comparison, including different geometries (pixelated and monolithic), surface finishes (for the lateral and back sides) and scintillation materials (LYSO and BGO). While changing the surface finish had little effect on the time resolution in monolithic LYSO due to already high photon collection efficiencies, it plays an important role in Cerenkov based time estimation for BGO due to much lower photon statistics. Surface finishes that improve photon collection efficiency result in time-of-flight kernels with shorter tails. Commonly used surface finishes in monolithic detectors (normally optimized for spatial resolution) result in inferior time resolution, showing potential benefit in making a switch to other surface finishes that increase photon collection efficiency such as reflective sides and a rough back surface.

Acknowledgements

The authors would like to thank Claudio Piemonte, Stefan Brunner and Tim Maximilian Fitzpatrick for their input on the SiPM simulation and preliminary results. The authors have no competing interests related to the content of this article. This work was funded by the Research Foundation Flanders, FWO (file number 79876 and Sphynx project).

References

Acerbi, Fabio and Stefan Gundacker (May 2019). “Understanding and simulating SiPMs”. en. In: *Nuclear Instruments and Methods in Physics Research*

Section A: Accelerators, Spectrometers, Detectors and Associated Equipment. Silicon Photomultipliers: Technology, Characterisation and Applications 926, pp. 16–35. ISSN: 0168-9002. DOI: 10.1016/j.nima.2018.11.118. URL: https://www.sciencedirect.com/science/article/pii/S0168900218317704 (visited on 08/25/2022).

AFBR-S4N66P024M 2×1 NUV-MT Silicon Photomultiplier Array (2022). Broadcom. URL: https://jp.broadcom.com/products/optical-sensors/silicon-photomultiplier-sipm/afbr-s4n66p024m.

Allison, J. et al. (Nov. 2016). "Recent developments in Geant4". en. In: *Nuclear Instruments and Methods in Physics Research Section A: Accelerators, Spectrometers, Detectors and Associated Equipment* 835, pp. 186–225. ISSN: 0168-9002. DOI: 10.1016/j.nima.2016.06.125. URL: https://www.sciencedirect.com/science/article/pii/S0168900216306957 (visited on 08/25/2022).

Berg, Eric, Emilie Roncali, and Simon R. Cherry (June 2015). "Optimizing light transport in scintillation crystals for time-of-flight PET: an experimental and optical Monte Carlo simulation study". EN. In: *Biomedical Optics Express* 6.6. Publisher: Optica Publishing Group, pp. 2220–2230. ISSN: 2156-7085. DOI: 10.1364/BOE.6.002220. URL: https://opg.optica.org/boe/abstract.cfm?uri=boe-6-6-2220 (visited on 10/12/2022).

BGO Scintillator (n.d.). Epic-Crystal. URL: https://www.epic-crystal.com/oxide-scintillators/bgo-scintillator.html.

Brunner, S. E. and D. R. Schaart (May 2017). "BGO as a hybrid scintillator / Cherenkov radiator for cost-effective time-of-flight PET". en. In: *Physics in Medicine & Biology* 62.11. Publisher: IOP Publishing, p. 4421. ISSN: 0031-9155. DOI: 10.1088/1361-6560/aa6a49. URL: https://iopscience.iop.org/article/10.1088/1361-6560/aa6a49/meta (visited on 09/08/2022).

Carra, Pietro et al. (June 2022). "A neural network-based algorithm for simultaneous event positioning and timestamping in monolithic scintillators". en. In: *Physics in Medicine & Biology* 67.13. Publisher: IOP Publishing, p. 135001. ISSN: 0031-9155. DOI: 10.1088/1361-6560/ac72f2. URL: https://dx.doi.org/10.1088/1361-6560/ac72f2 (visited on 11/22/2022).

Decuyper, Milan (2021). "Advancing medical imaging with artificial intelligence : PET acquisition enhancement and MRI-based brain tumour diagnosis". eng. PhD thesis. Ghent University, XXXII, 307. ISBN: 9789463555364.

Dietz-Laursonn, Erik (Dec. 2016). *Peculiarities in the Simulation of Optical Physics with Geant4*. arXiv:1612.05162 [physics]. DOI: 10.48550/arXiv.1612.05162. URL: http://arxiv.org/abs/1612.05162 (visited on 08/22/2022).

Efthimiou, Nikos et al. (Sept. 2021). "TOF-PET Image Reconstruction With Multiple Timing Kernels Applied on Cherenkov Radiation in BGO". In: *IEEE Transactions on Radiation and Plasma Medical Sciences* 5.5. Conference Name: IEEE Transactions on Radiation and Plasma Medical Sciences, pp. 703–711. ISSN: 2469-7303. DOI: 10.1109/TRPMS.2020.3048642.

Gonzalez-Montoro, Andrea et al. (May 2021). "Evolution of PET Detectors and Event Positioning Algorithms Using Monolithic Scintillation Crystals". In: *IEEE Transactions on Radiation and Plasma Medical Sciences* 5.3. Conference Name: IEEE Transactions on Radiation and Plasma Medical Sciences, pp. 282–305. ISSN: 2469-7303. DOI: 10.1109/TRPMS.2021.3059181.

Gundacker, Stefan et al. (Jan. 2020). "Experimental time resolution limits of modern SiPMs and TOF-PET detectors exploring different scintillators and Cherenkov emission". en. In: *Physics in Medicine & Biology* 65.2. Publisher: IOP Publishing, p. 025001. ISSN: 0031-9155. DOI: 10.1088/1361-6560/ab63b4. URL: https://doi.org/10.1088/1361-6560/ab63b4 (visited on 08/03/2022).

Jarron, P. et al. (Oct. 2009). "Time based readout of a silicon photomultiplier (SiPM) for time of flight positron emission tomography (TOF-PET)". In: *2009 IEEE Nuclear Science Symposium Conference Record (NSS/MIC)*. ISSN: 1082-3654, pp. 1212–1219. DOI: 10.1109/NSSMIC.2009.5402391.

Kratochwil, Nicolaus et al. (June 2020). "Pushing Cherenkov PET with BGO via coincidence time resolution classification and correction". en. In: *Physics in Medicine & Biology* 65.11. Publisher: IOP Publishing, p. 115004. ISSN: 0031-9155. DOI: 10.1088/1361-6560/ab87f9. URL: https://doi.org/10.1088/1361-6560/ab87f9 (visited on 10/12/2022).

Krishnamoorthy, Srilalan et al. (July 2018). "Performance evaluation of the MOLECUBES β-CUBE—a high spatial resolution and high sensitivity small animal PET scanner utilizing monolithic LYSO scintillation detectors". en. In: *Physics in Medicine & Biology* 63.15. Publisher: IOP Publishing, p. 155013. ISSN: 0031-9155. DOI: 10.1088/1361-6560/aacec3. URL: https://dx.doi.org/10.1088/1361-6560/aacec3 (visited on 11/22/2022).

LYSO(Ce) Scintillator (n.d.). Epic-Crystal. URL: https://www.epic-crystal.com/oxide-scintillators/lyso-ce-scintillator.html.

Roncali, Emilie and Simon R. Cherry (Mar. 2013). "Simulation of light transport in scintillators based on 3D characterization of crystal surfaces". en. In: *Physics in Medicine & Biology* 58.7. Publisher: IOP Publishing, p. 2185. ISSN: 0031-9155. DOI: 10.1088/0031-9155/58/7/2185. URL: https://iopscience.iop.org/article/10.1088/0031-9155/58/7/2185/meta (visited on 08/25/2022).

Sánchez, David et al. (Jan. 2022). "HRFlexToT: A High Dynamic Range ASIC for Time-of-Flight Positron Emission Tomography". In: *IEEE Transactions on Radiation and Plasma Medical Sciences* 6.1. Conference Name: IEEE Transactions on Radiation and Plasma Medical Sciences, pp. 51–67. ISSN: 2469-7303. DOI: 10.1109/TRPMS.2021.3066426.

Sarrut, David et al. (May 2021). "Advanced Monte Carlo simulations of emission tomography imaging systems with GATE". en. In: *Physics in Medicine & Biology* 66.10. Publisher: IOP Publishing, 10TR03. ISSN: 0031-9155. DOI: 10.1088/1361-6560/abf276. URL: https://iopscience.iop.org/article/10.1088/1361-6560/abf276/meta (visited on 08/25/2022).

Shinotsuka, H. et al. (2015). "Calculations of electron inelastic mean free paths. X. Data for 41 elemental solids over the 50 eV to 200 keV range with the relativistic full Penn algorithm". en. In: *Surface and Interface Analysis* 47.9. _eprint: https://onlinelibrary.wiley.com/doi/pdf/10.1002/sia.5789, pp. 871–888. ISSN: 1096-9918. DOI: 10.1002/sia.5789. URL: https://onlinelibrary.wiley.com/doi/abs/10.1002/sia.5789 (visited on 06/16/2022).

Stockhoff, Mariele et al. (July 2021). "High-resolution monolithic LYSO detector with 6-layer depth-of-interaction for clinical PET". en. In: *Physics in Medicine & Biology* 66.15. Publisher: IOP Publishing, p. 155014. ISSN: 0031-

9155. DOI: 10.1088/1361-6560/ac1459. URL: https://iopscience.iop.org/article/10.1088/1361-6560/ac1459/meta (visited on 09/09/2022).

Trigila, Carlotta, Gerard Ariño-Estrada, et al. (2022). "The Accuracy of Cerenkov Photons Simulation in Geant4/Gate Depends on the Parameterization of Primary Electron Propagation". In: *Frontiers in Physics* 10. ISSN: 2296-424X. URL: https://www.frontiersin.org/article/10.3389/fphy.2022.891602 (visited on 06/16/2022).

Trigila, Carlotta, Eshani Moghe, and Emilie Roncali (2021). "Technical Note: Standalone application to generate custom reflectance Look-Up Table for advanced optical Monte Carlo simulation in GATE/Geant4". en. In: *Medical Physics* 48.6. _eprint: https://onlinelibrary.wiley.com/doi/pdf/10.1002/mp.14863, pp. 2800–2808. ISSN: 2473-4209. DOI: 10.1002/mp.14863. URL: https://onlinelibrary.wiley.com/doi/abs/10.1002/mp.14863 (visited on 11/18/2022).

Vandenberghe, Stefaan et al. (2022). "Efficient patient throughput and detector usage in low cost efficient Monolithic High resolution Walk-through Flat Panel Total Body PET". und. In: Edinburgh: Total-Body PET conference. URL: https://totalbodypet2020org.files.wordpress.com/2022/09/online_conference_booklet_final.pdf.